Original Article

Institution of MECHANICAL ENGINEERS
Journal of RAIL AND RAPID TRANSIT

Proc IMechE Part F:
J Rail and Rapid Transit
0(0) 1–15

DOI: 10.1177/0954409718810262
journals.sagepub.com/home/pif
SAGE

# Field investigation and full-scale model testing of mud pumping and its effect on the dynamic properties of the slab track–subgrade interface

**Junjie Huang[1,2], Qian Su[1,2], Wei Wang[1,2], Pham Duc Phong[3] and Kaiwen Liu[1,2]**

## Abstract

Passenger comfort and safety are the most important aspects in the operation of high-speed railways. Mud pumping is a typical problem that occurs in the slab track and the subgrade interface, which influences passenger comfort and safety. In this paper, various field investigations and a full-scale model of the slab track and the subgrade are presented. The external and internal characteristics of mud pumping in the slab track–subgrade interface and the influence of mud pumping on the dynamic properties of the slab track–subgrade are analyzed. The results show that mud pumping only occurs at the expansion joints in the concrete base of the slab track structure. This happens due to the infiltration of rainwater into the subgrade bed through the cracks in the expansion joints. When the upper layer of the subgrade is kept saturated in the full-scale model, mud pumping is found to occur after $3.0 \times 10^4$ loading cycles. The vibration ratio of the subgrade surface to the concrete base gradually increases with continued cyclic loading. In addition, the cumulative settlement of the subgrade increased continuously. After $2.0 \times 10^6$ loading cycles, it was found that a large volume of slurry composed of water and fine particles was squeezed out of the subgrade bed, and mud pumping occurred on the surface of the subgrade bed leading to the formation of a mud layer between the concrete base and the subgrade bed, causing a loss of contact between the subgrade bed and the concrete base. This reduces the ability of the subgrade bed to support the slab track structure.

## Keywords

High-speed railway, slab track structure, subgrade bed, field investigation, full-scale model, mud pumping, dynamic properties

Date received: 2 December 2016; accepted: 6 October 2018

## Introduction

The subgrade mainly consists of the subgrade filling layer, and the lower and the upper layers of the subgrade bed from bottom to top serve as the foundation for supporting the slab track structure. The subgrade should have enough strength, appropriate stiffness, and long-term stability to handle the vehicle dynamic loads, and to ensure the safety and comfort of operation of high-speed railways.[1–4] Therefore, there are extremely high requirements for the design, construction, and maintenance of the subgrade under the slab track structure. However, under operational conditions, the subgrade is affected by temperature, rainwater, and vehicle dynamic loads, and a significant dynamic coupling effect is found to occur in the slab track–subgrade system under high-speed moving train load.[5–11]

With the increase in the operating speeds of high-speed railways, many researchers are focussing more attention on the slab track–subgrade, where many 2.5D and 3D finite element models, train–track–ground integrated dynamic model, full-scale models, and even large-scale international testing are

[1]Key Laboratory of High-Speed Railway Engineering of Ministry of Education, Southwest Jiaotong University, Chengdu, China
[2]School of Civil Engineering, Southwest Jiaotong University, Chengdu, China
[3]Institute of Techniques for Special Engineering, Le Quy Don Technical University, Hanoi, Vietnam

**Corresponding author:**
Qian Su, Key Laboratory of High-Speed Railway Engineering of Ministry of Education, Southwest Jiaotong University, No. 111 First Section, North of Second Ring Road, Chengdu 610031, Sichuan, China.
Email: suqian@126.com

performed to analyze the dynamic properties and vibrations of the slab track–subgrade under train load.[12–18] These studies indicate that the slab track–subgrade has good long-term dynamic stability when the performance of the slab track–subgrade cannot be deteriorated by poor construction quality, temperature, and rainwater. However, the slab track–subgrade is prone to damages, such as cracks in the interlayers of the slab track–subgrade and the waterproof seal layer due to temperature and material aging. During rainy season, rainwater infiltrates into the subgrade bed through the cracks, which causes the subgrade bed to be affected by the dynamic fluid–solid coupling effect. With the increase in the operational time of high-speed railways, some mud pumping cases are found to occur in the slab track–subgrade. Nowadays, mud pumping of the slab track–subgrade is the most typical damage that directly affects the operational comfort and safety of high-speed railways.

In the field of highway, many researchers have analyzed the formation mechanisms and variations of pore water pressure and the fine particle migration in the interlayer between pavement and subgrade, based on a variety of indoor and outdoor experiments and on-site tests. The same researches are performed in the ballast bed under the track. These studies show that the formation and dissipation processes of pore water pressure have an important influence on the fine particle migration, which causes mud pumping in the highway subgrade and the ballast bed.[19–24] In order to improve the resistance to mud pumping that occurs in the sub-base of the pavement and the ballast bed of railways, some reinforced methods and remedial measures including the sub-base and subgrade mixed with cement and reinforced with geosynthetics (geogrid, geocell, and geotextile) have been proposed in fields of highway and traditional ballast track.[25–30] However, only a few researchers have focused on mud pumping and its remediations of the slab track–subgrade of high-speed railways. According to these studies, mud pumping and its effect on the dynamic properties of the slab track–subgrade of high-speed railway differ from that of the ballast bed under conventional ballast track and the sub-base of pavement owing to some differences in loading condition and structural characteristics between the slab track–subgrade and the conventional ballast track and highway subgrade. Under high-speed train load, occurrence of mud pumping in the slab track–subgrade can impel the fine particles in the upper layer of subgrade bed to migrate and squeeze out of the subgrade bed, which causes the reduction of the supporting capability of the subgrade bed to the slab track structure, the longitudinal uneven of subgrade bed stiffness to the slab track, and intensified vibration of the slab track structure.[31–36] Presently, the study on the mud pumping characteristics and mechanisms of the slab track–subgrade has not yet attracted much attention of researchers. However, with the increase in the operational time of the slab track–subgrade of high-speed railways, gradually there will be more and more occurrences of mud pumping of the slab track–subgrade, which will then be one of the key factors threatening the operational comfort and safety of high-speed railways. Thus, while mud pumping of the slab track–subgrade has not yet become an important issue affecting the comfort and safety of high-speed railways, researchers and operational management departments of high-speed railways should put greater impetus on studying the mechanisms and characteristics of the occurrence of mud pumping in the slab track–subgrade, so as to provide a basis for the optimum structural design and maintenance of the slab track–subgrade.

In this paper, various field investigations were conducted to analyze the mud pumping characteristics of the slab track–subgrade of high-speed railways during operation. Then, a full-scale model of the slab track–subgrade was established to analyze the characteristics of mud pumping in the subgrade bed and its effect on the dynamic properties of the slab track–subgrade under cyclic dynamic load when the graded crush stone in the subgrade bed is saturated by water.

## Field investigation on mud pumping

The field investigations only focus on the subgrade sections of the high-speed railway line, which are paved by the China Railway Track System (CRTS) I slab track structure, as shown in Figure 1. The slab track–subgrade mainly consists of the slab track structure, the upper and lower layers of the subgrade bed, and the common subgrade filling layer from top to bottom. The thickness of the upper layer of the subgrade bed is 0.4 m at the subgrade center. The interface between the upper and lower layers of the subgrade bed is a slope with 4% in the lateral direction, as shown in Figure 1(a).

In order to overcome the expansion deformation of the concrete base induced by differential temperature, the concrete base has an expansion joint at regular intervals along the line, the regular intervals of CRTS I slab track structure are 20.108 m, as shown in Figure 1(b). All the expansion joints have to be filled with waterproof materials to prevent rainwater from infiltrating into the subgrade bed. The slab track structure is placed on the subgrade bed consisting of the upper layer with a width of 0.4 m and the lower layer with a width of 2.3 m. Traditionally, the upper and lower layers of the subgrade bed are filled with the graded crush stone and the group A or B packing, respectively.[37] The upper layer of the subgrade bed is significantly affected by the high-speed train load in comparison with the lower layer of the subgrade bed and the common subgrade filling layer. According to a series of on-site tests, the dynamic soil pressure in the upper layer of the subgrade bed is in the

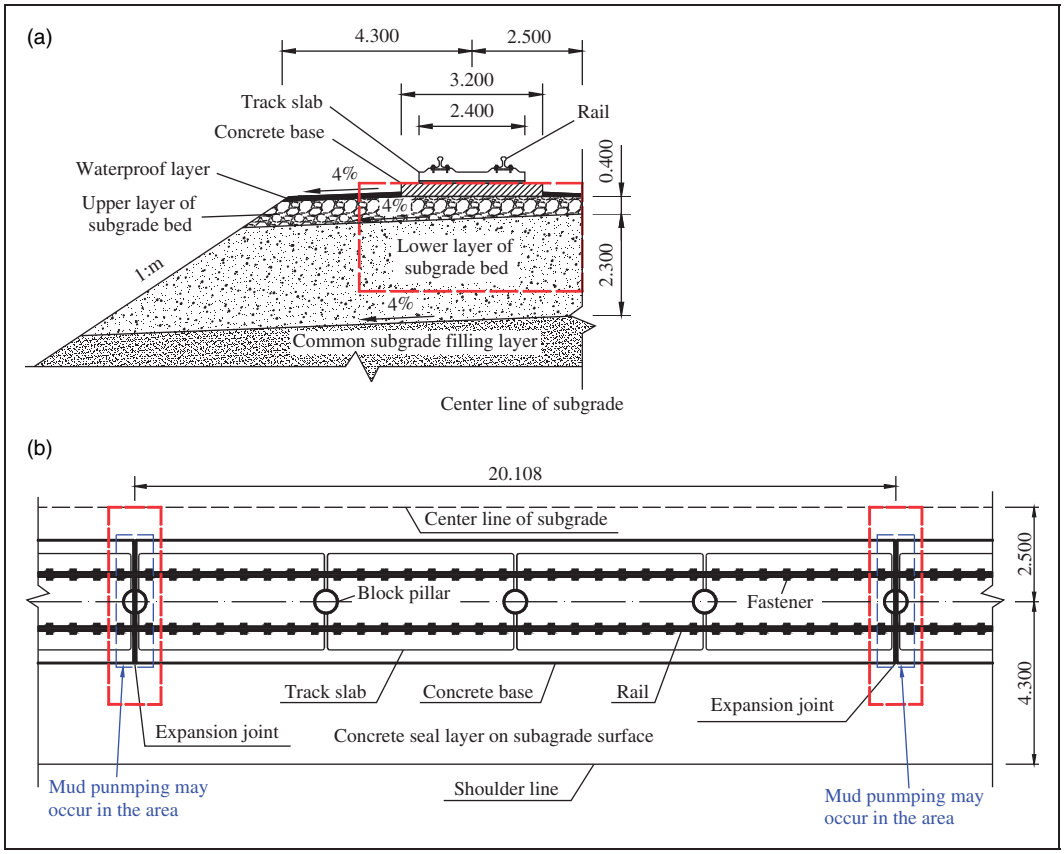


**Figure 1.** The structural characteristics of the slab track–subgrade (unit in m): (a) the cross-sectional profile of the slab track–subgrade; (b) the plane section of the slab track–subgrade.

range of 13–40 kPa under high-speed moving train load,[9–12,38–43] which is less than the design value of 100 kPa.[37] After the slab track–subgrade is put into operation for several years, there are some cases of mud pumping occurring in the slab track–subgrade, causing stiffness irregularities of the slab track–subgrade.

In this paper, a variety of field investigations were carried out to analyze the mud pumping characteristics of the slab track–subgrade. Firstly, various field investigations based on visual observation mainly focus on the mud pumping location along the railway line and its characteristics in the slab track–subgrade. The results of these field investigations are listed as follows:

(1) Mud pumping only occurs in the expansion joints of the concrete base of the slab track structure, as shown in Figure 2. This is because cracks occur in the expansion joints due to the waterproof materials in the expansion joint aging, which causes rainwater to infiltrate into subgrade bed through the cracks during rainy season.
(2) Under high-speed moving train during the rainy season, a large volume of slurry is squeezed out of the subgrade bed from the cracks in the expansion joint of the concrete base, as shown in Figure 2(a). A large number of fine particles are carried out through water expelled from the subgrade bed and lay on the waterproof seal layer of the subgrade, as shown in Figure 2(b).

Secondly, the ground-penetrating radar and impact-echo method are used to detect mud pumping in the slab track–subgrade, as shown in Figure 3. Due to several layers of reinforcing steel rebars in the slab track structure, the electromagnetic wave cannot pass and reflect through the slab track structure,[44,45] and therefore, the ground penetrating radar is not suitable for detecting mud pumping in the interlayer between the concrete base and subgrade bed. But the ground penetrating radar can accurately test areas outside of the concrete base because of the concrete waterproof layer without reinforcing steel rebars.[46,47] The impact-echo method, which is an effective nondestructive testing technique widely used for detecting certain defects inside concrete elements or structures based on the frequency spectrum analysis,[48,49] is introduced to detect the occurrence of mud pumping in the subgrade bed under the slab track structure, because there are different supporting conditions of the subgrade bed to the slab track structure under mud pumping occurring in the subgrade bed or not.

Based on the impact-echo method and the ground penetrating radar used for measuring the internal characteristics of mud pumping in the subgrade bed,

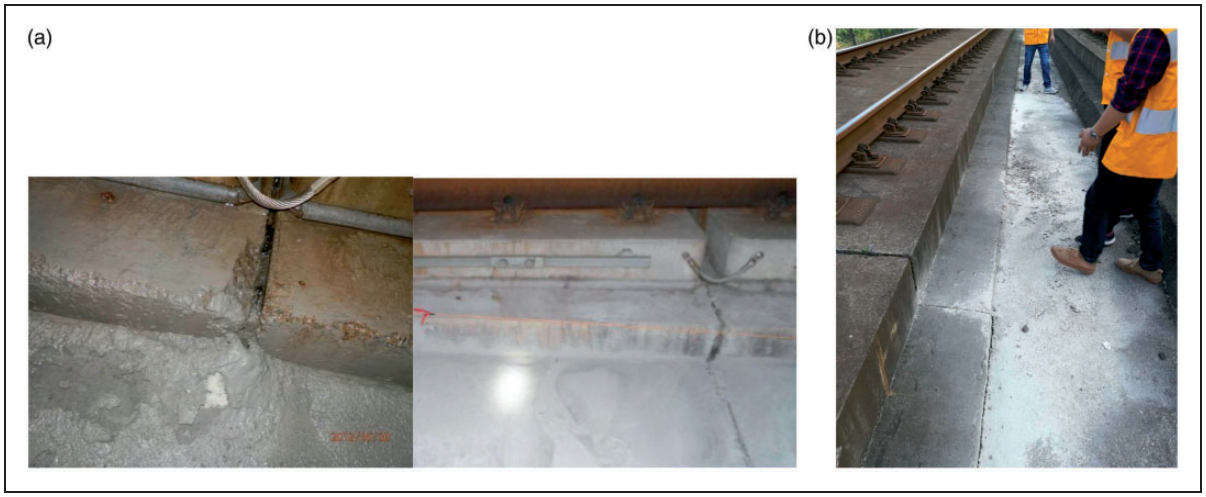


**Figure 2.** The external characteristics of mud pumping occurring in the slab track–subgrade during operation: (a) slurries squeezed out during the rainy season; (b) fine particles during the dry season.


**Figure 3.** Ground penetrating radar and impact-echo method for detecting mud pumping: (a) ground penetrating radar analyzing the subgrade surface; (b) analysis of the slab track structure by the impact-echo method.

it is found that mud pumping only occurs in areas below the width of the concrete base and near the expansion joints in the longitudinal direction. Mud pumping can deteriorate with the increase of coupling effects of high-speed moving train loads and rainwater, leading to a reduction of the supporting capability of the subgrade bed to the slab track due to fine particles moving out of the subgrade bed. Therefore, mud pumping has to be reinforced in a timely manner during operation.

According to various field investigations, the main reason for mud pumping in the slab track–subgrade is that rainwater infiltrates into subgrade bed through cracks in the expansion joint of the concrete base. Under high-speed moving train load, the graded crush stone in the upper layer of the subgrade bed is affected by the dynamic fluid–solid coupling effects, causing the migration of fine particles of the graded crush stone. Especially, the fine particles are carried out of the subgrade bed in the process of the rainwater pumping (Figure 2). The reduction of fine particles in the subgrade bed and the graded crush stone affected by rainwater can reduce the supporting capability of the subgrade bed to the track structure. However, the internal characteristics of mud pumping in the subgrade bed and the influence of mud pumping on the dynamic properties of the slab track–subgrade are still unknown. Therefore, a full-scale experimental model consisting of the concrete base and subgrade bed is established in this paper.

## Full-scale model test

### *Establishment of the full-scale model*

According to the structural characteristics of the slab track–subgrade (Figure 1), a full-scale model of the slab track–subgrade is established, as shown

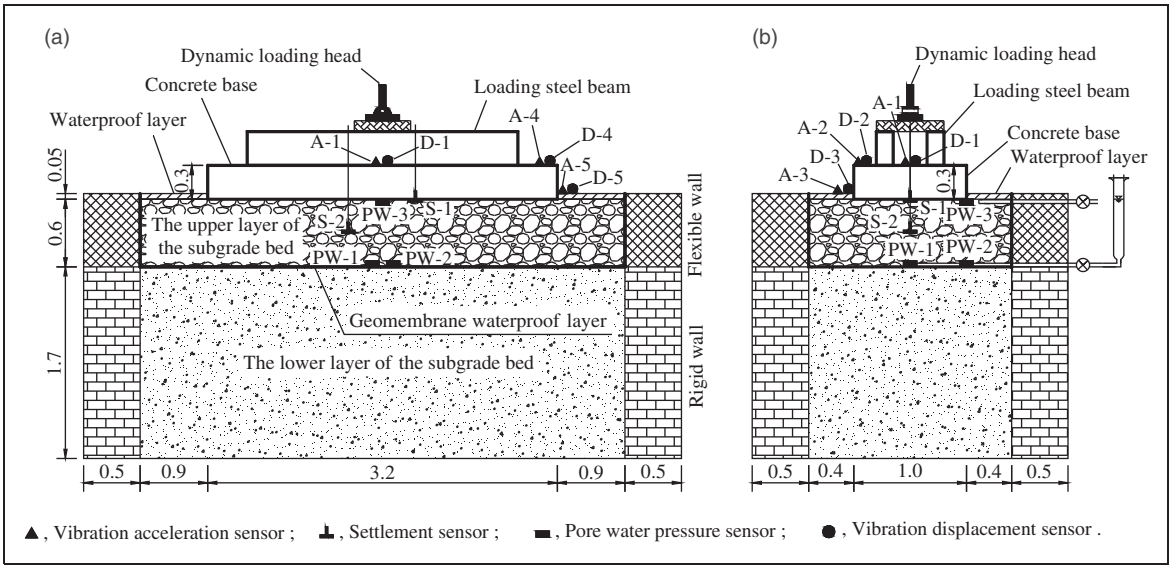


**Figure 4.** A full-scale model of the slab track–subgrade: (a) cross-sectional view; (b) longitudinal section view (unit in m).

in Figure 4. Based on the structural optimization of the slab track–subgrade located in the area of the red dashed boxes (Figure 1), the full-scale model mainly consists of the concrete base, and the upper and lower layers of subgrade bed from top to bottom. In order to simulate the infiltration of rainwater into subgrade bed and its gathering in there, a waterproof layer composed of geomembrane is installed between the upper and lower layers of the subgrade bed and wrapped around the side of the upper layer of the subgrade bed, so that the upper layer of the subgrade bed can be saturated by water.

The slab track–subgrade within the red dashed boxes in Figure 1 has an expansion joint of the concrete base in the middle. Rainwater infiltrates into the subgrade bed from cracks in the expansion joint and the slurries are squeezed out from that. In this full-scale model test, the purpose of this study is not to focus on the way the rainwater and slurries are squeezed out of the subgrade bed, but to analyze the internal characteristics of mud pumping and its influences on the dynamic properties of the slab track–subgrade under the upper layer of the subgrade bed saturated by water. Therefore, the slab track structure can be simplified to one layer of the concrete base with a width of 3.20 m in the horizontal direction and length of 1.00 m in the longitudinal direction. The subgrade bed mainly consists of the upper and lower layers with the thickness of 0.60 m and 1.70 m, respectively.

The upper and lower layers of the subgrade bed are filled with the graded crush stone and the group A packing, respectively. Before the graded crush stone and group A packing are used to fill the model, a series of sieve tests are conducted on the graded distribution according to the Chinese specification for soil test of railway engineering.[50] The nonuniform coefficient $C_u$ and curvature coefficient $C_c$ of the group A packing and graded crush stone are listed in Table 1. The grain-size distribution curve of the graded crush stone is shown in Figure 5.

**Table 1.** Gradation indexes of the graded crush stone and group A packing.

| Gradation indexes | Graded crush stone | Group A packing |
|---|---|---|
| $C_u$ | 27.80 | 22.47 |
| $C_c$ | 1.05 | 2.05 |

The nonuniform coefficients $C_u$ of the graded crush stone and group A packing are more than 15, and their curvature coefficients $C_c$ are between 1 and 3. The results show that the nonuniform coefficient and curvature coefficients of the graded crush stone and group A packing, and grain-size distribution of graded crush stone meet the requirements of the Chinese design specification.[37] Therefore, the graded crush stone and group A packing, which are configured with the optimum water content of 5.22% and 4.58% from various compaction tests respectively, can be used to fill the upper and lower layers of the subgrade bed, as shown in Figure 6. In the filling process of the model, compaction quality of the graded crush stone and group A packing has to be rigorously tested. The test items are foundation coefficient $K_{30}$, dynamic deformation module $E_{vd}$, and compaction coefficient $K$. The detection process of these test items is conducted according to the Chinese specification for soil test of railway engineering.[50] The test results are listed in Table 2.

## Loading procedures

A large-scale loading test system, which can output a sine wave load with the load amplitude of 0–250 kN

and load frequency of 0–10 Hz, is used to supply the cyclic dynamic load on the model. Under high-speed moving train load, the amplitude of the dynamic soil stress at the upper surface of the subgrade bed is mainly in the range of 13–24 kPa based on various field measurements,[9–12,38–43] which is less than the design value of 100 kPa.[37] The frequency of the dynamic soil stress responses on the subgrade bed surface are mainly determined by the speed and axle spacing of a moving train. Most of the powers of the dynamic soil stresses on the subgrade bed surface are concentrated at a frequency of less than 15 Hz.[38–43] For example, when the speed of train is 330 km/h, the dominant frequency is about 3.6 Hz and 11.1 Hz corresponding to the length of a carriage (25 m) and the distance of two bogies in the adjacent carriages (7.5 m).[42,43] Therefore, according to the loading capacity of the large-scale loading test system, a cyclic dynamic load with the upper limit of 96 kN and frequency of 5 Hz, which is determined according to the above field measurements, is applied on the beam above the concrete base of the model. The dynamic soil stress on the subgrade bed surface of the model is in the range of 25–30 kPa under the cyclic dynamic loading output from the system.

The cyclic dynamic loading procedures for the full-scale model are divided into two stages, as follows.

(1) In the first stage, the cyclic dynamic loading of $2.0 \times 10^6$ cycles is applied to the loading steel beam to simulate the slab track subgrade put into operation after the construction of the full-scale model is completed. In this stage, the graded crushed stone of the upper layer of the subgrade bed is in the optimum water content.
(2) In the second stage, once the first loading stage is completed, the graded crush stone in the upper layer of the subgrade bed is injected and immersed by water until saturation. Then another $2.0 \times 10^6$ cycles are continually applied to the full-scale model.

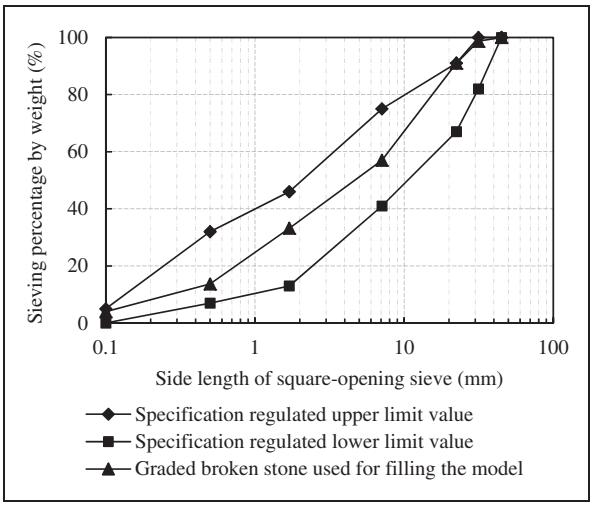


**Figure 5.** Grain-size distribution curve of the graded crush stone.

## Test items

The test items include the vertical vibration acceleration and displacement of the concrete base and subgrade surface close to the concrete base, and the cumulative settlement and the pore pressure of the

**Table 2.** Results of the investigation of the compaction quality of the subgrade bed and the compaction standard.

| | $K_{30}$ (MPa/m) | | $E_{vd}$ (MPa) | | $K$ | |
|---|---|---|---|---|---|---|
| Layer name | Tested value | Standard value | Tested value | Standard value | Tested value | Standard value |
| Lower layer | ⩾220 | ⩾130 | ⩾95 | ⩾40 | ⩾0.95 | ⩾0.95 |
| Upper layer | ⩾255 | ⩾190 | ⩾120 | ⩾55 | ⩾0.97 | ⩾0.97 |

**Figure 6.** The graded crush stone in the optimum water content used to fill the upper layer of subgrade bed.

upper layer of the subgrade bed. All the sensors are installed according to the corresponding positions shown in Figure 4. Some sensors testing for vibration of the concrete base and subgrade surface are shown in Figure 7. During the loading process of the full-scale model, the signals of all the sensors are collected by a dynamic acquisition system. Then the collective voltage signals of all the sensors are converted into the vibration acceleration and displacement, and settlement datum by the corresponding process software installed in the dynamic acquisition system, which has amplification, filtering, and sampling functions for the collective voltage signals.

## Analysis of the experimental results

### *Vertical vibration acceleration*

When the upper layer of the subgrade bed is in normal condition (optimum water content), the variation of the vertical vibration acceleration of the slab track–subgrade with the number of loading cycles are is shown in Figure 8(a). The vertical vibration acceleration is the amplitude value in each loading cycle. During early loading stage, the vertical vibration acceleration of the concrete base decreases gradually, and that of the subgrade bed surface increases gradually. Both tend to be stable as soon as the number of loading cycles reaches $8.0 \times 10^5$ times.

With the upper layer of the subgrade bed saturated by water, the variation of the vertical vibration acceleration of the concrete base and subgrade surface close to the concrete base with the number of loading cycles is as shown in Figure 8(b). The vertical vibration acceleration of the concrete base increases quickly when the number of loading cycles is less than $8.0 \times 10^5$ times, and then increases gradually with the increase of the loading times because mud pumping begins to occur in the full-scale model after $3.0 \times 10^4$ cycles. However, the vertical vibration acceleration of the subgrade surface decreases slightly with the increasing number of loading cycles.

After $5.0 \times 10^5$ cycles in each loading stage, the time–history curves of the vertical vibration acceleration of test points A1 at the concrete base center and A3 at the subgrade surface are as shown in Figures 9 and 10, while the upper layer of the subgrade bed is in the normal and mud pumping conditions, respectively.

When the upper layer of the subgrade bed is in the normal condition, the average value of the measuring-point A1 on the concrete base in 3 s is 0.332 m/s$^2$; and that of the measuring-point A3 on the subgrade surface is 0.146 m/s$^2$. After the upper layer of the subgrade bed is saturated by water in the second loading stage, the former is 0.582 m/s$^2$, the latter is 0.050 m/s$^2$. Obviously, the average amplitude value of the vertical vibration acceleration of the concrete base under the upper layer of the subgrade bed saturated by water increases by 75.3% in comparison with the upper

**Figure 7.** Installation of the testing sensors in the full-scale model.

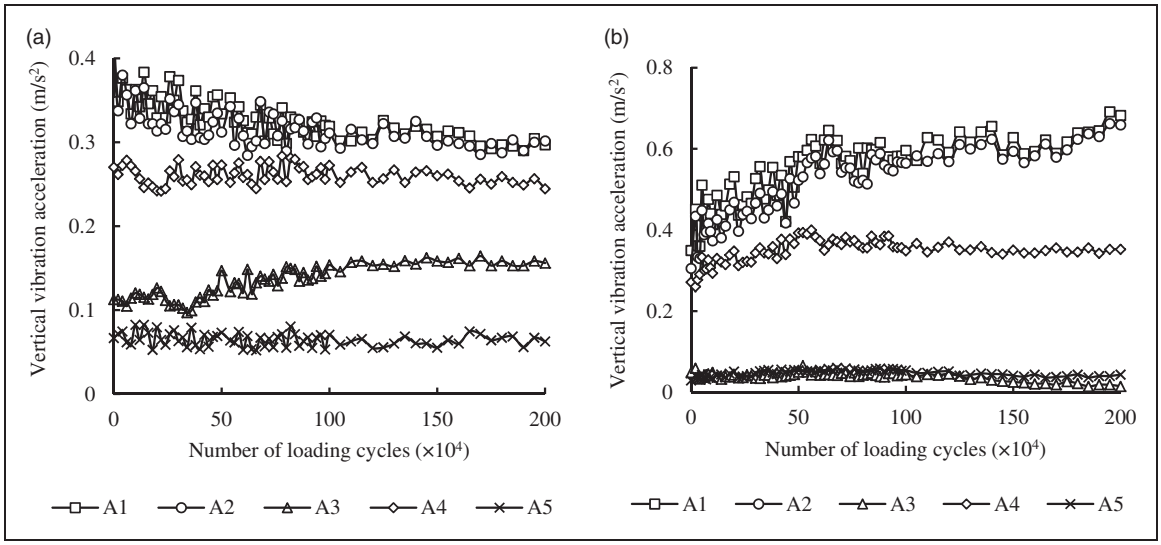


**Figure 8.** The variation of the vertical vibration acceleration with the number of loading cycles: (a) the upper layer of the subgrade bed in the normal condition; (b) the upper layer of subgrade bed in the saturation condition.

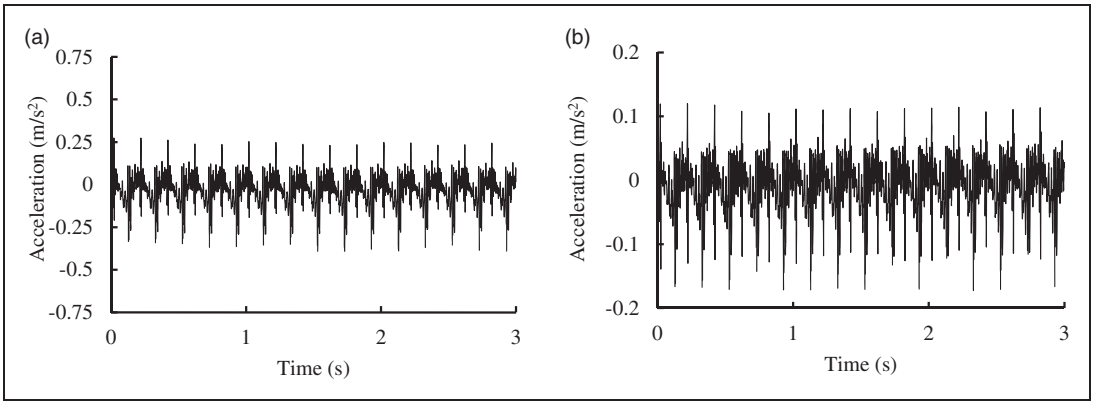


**Figure 9.** The time–history curve of the vertical vibration acceleration under the upper layer in the normal condition: (a) measuring-point A1; (b) measuring-point A3.

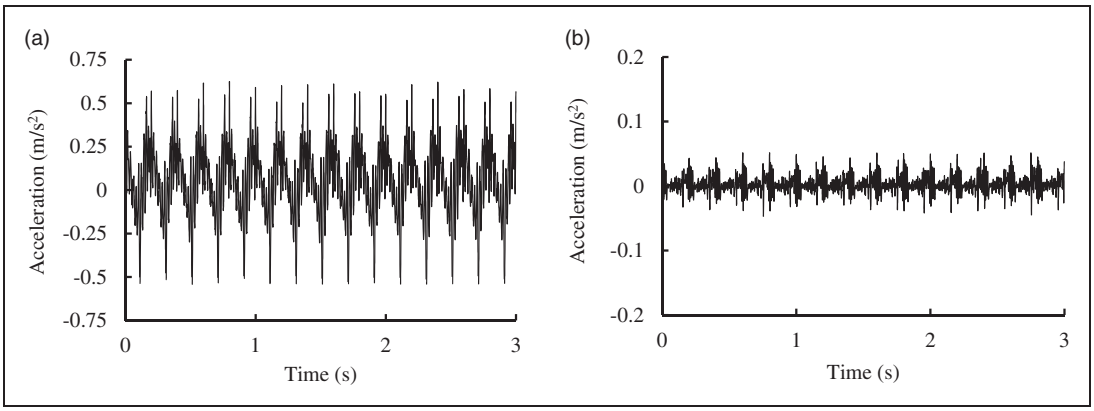


**Figure 10.** The time–history curve of the vertical vibration acceleration under the upper layer in the saturation condition: (a) measuring-point A1; (b) measuring-point A3.

layer of the subgrade bed in normal condition, while that of the subgrade surface close to the concrete base reduces by 65.8%.

When the upper layer of the subgrade bed is in normal and saturation conditions, the ratios of the vertical vibration acceleration of measuring-points A1 and A3 after the completion of both the loading stages are 1.90:1 and 46.09:1, respectively. In the second loading stage, some slurries begin to be squeezed out of the subgrade bed after $3.0 \times 10^4$ cycles, as shown in Figure 11(a), and mud pumping begins to occur in the full-scale model. Mud pumping in the subgrade bed gradually deteriorates with the increasing number of loading cycles, which causes a large volume of slurry to be squeezed out of the subgrade bed, as shown in Figure 11(b). Based on the variation of vibration of the model with the number of loading cycles for the upper layer of the subgrade bed in normal and saturation conditions, the occurrence of mud pumping in the subgrade bed can significantly intensify the vibration of the slab track–subgrade, which affects the comfort and safety of operation of high-speed railways.

### *Vertical vibration displacement*

Under cyclic dynamic load, the variation of the vertical vibration displacement of the concrete base and subgrade surface with the number of loading cycles is as shown in Figure 12, when the upper layer of the subgrade bed is in normal and saturation conditions, respectively.

When the upper layer of the subgrade bed is in the normal condition, the vertical vibration displacement of the concrete base and subgrade surface close to the concrete base gradually stabilizes with the increasing number of loading cycles. While the upper layer of the subgrade bed is in the saturation condition, the vertical vibration displacement of the concrete base increases quickly when the number of loading cycles is no more than $8.0 \times 10^5$ times, and then increases gradually until all the loading cycles of the second loading stage is completed; however, the vertical vibration displacement of the subgrade surface close to the concrete base tends to stabilize after a quick decreasing trend.

When the upper layer of the subgrade bed is in normal and saturation conditions, after $2.0 \times 10^6$

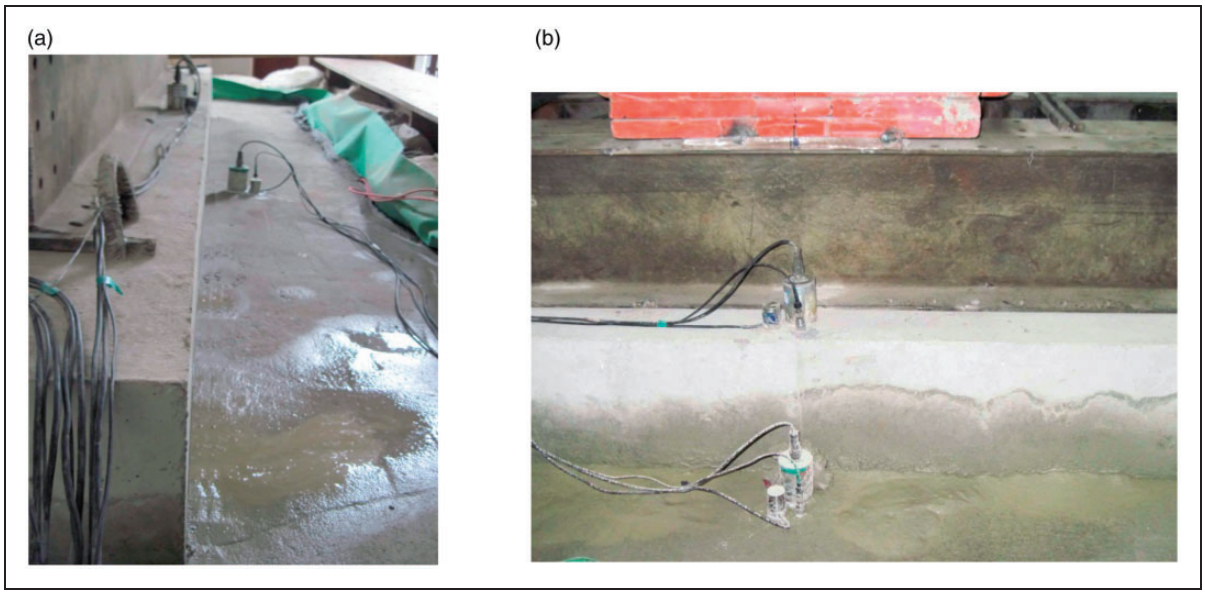


**Figure 11.** The characteristics of the occurrence of mud pumping in the model in the process of cyclic loading: (a) the initial stage of mud pumping; (b) the serious deterioration stage of mud pumping.

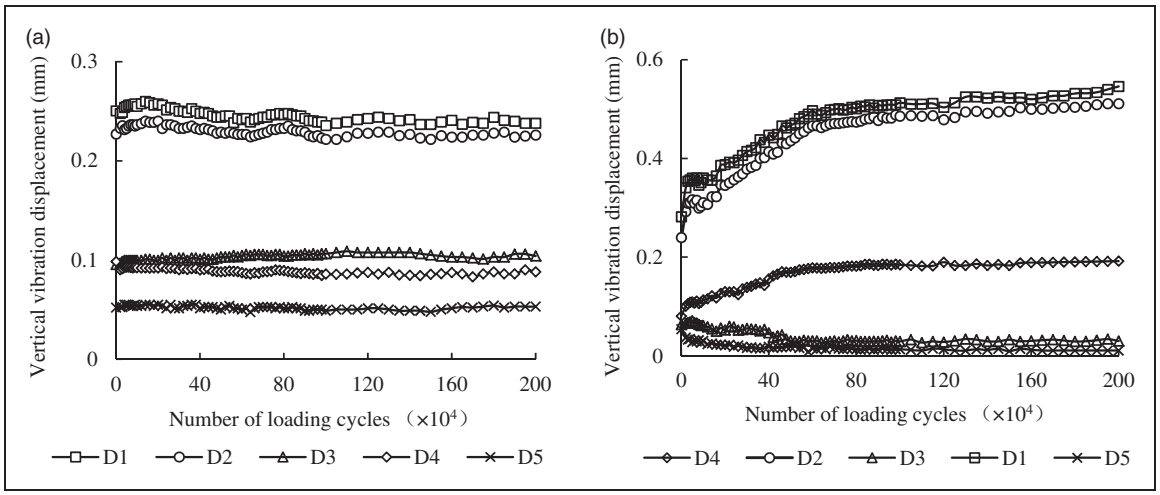


**Figure 12.** The variation of the vertical vibration displacement with the number of loading cycles: (a) the upper layer of subgrade bed in the normal condition; (b) the upper layer of subgrade bed in the saturation condition.

cycles the vertical vibration displacement of the concrete base center is found to be 0.238 mm and 0.549 mm, respectively; and that of the subgrade surface close to the concrete base (measuring-point A3) is 0.104 mm and 0.030 mm, respectively. With the upper layer of the subgrade bed saturated by water, the vertical vibration displacement of the concrete base center increases by 130.7% in comparison with the upper layer of the subgrade bed in the normal condition, while that of the subgrade surface (measuring-point A3) close to the concrete base reduces by 71.1%. When the upper layer of the subgrade bed is in normal and saturation conditions, the ratios of the vertical vibration displacement of measuring-point A1 on the concrete base center to that of measuring-point A3 on the subgrade surface close to the concrete base are 2.17:1 and 18.32:1, respectively.

With the increasing number of loading cycles, the variation of the vertical vibration displacement of the model is basically similar to the variation of the vertical vibration acceleration of the model, when the upper layer of the subgrade bed is in normal and saturation conditions, respectively. After the upper layer of the subgrade bed is saturated by water, mud pumping occurs in the subgrade bed under cyclic loading and deteriorates with the increasing number of loading cycles, which causes the intensification of the vibration of the model.

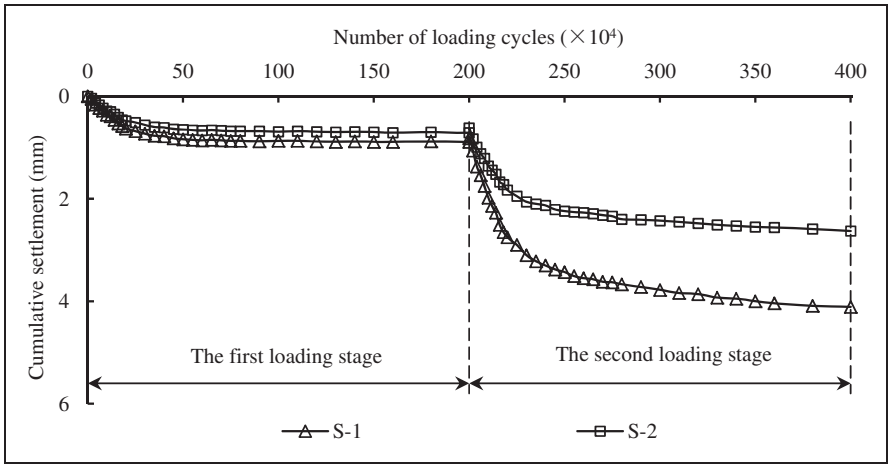


**Figure 13.** The variation of the cumulative settlement of the subgrade bed with the number of loading cycles.

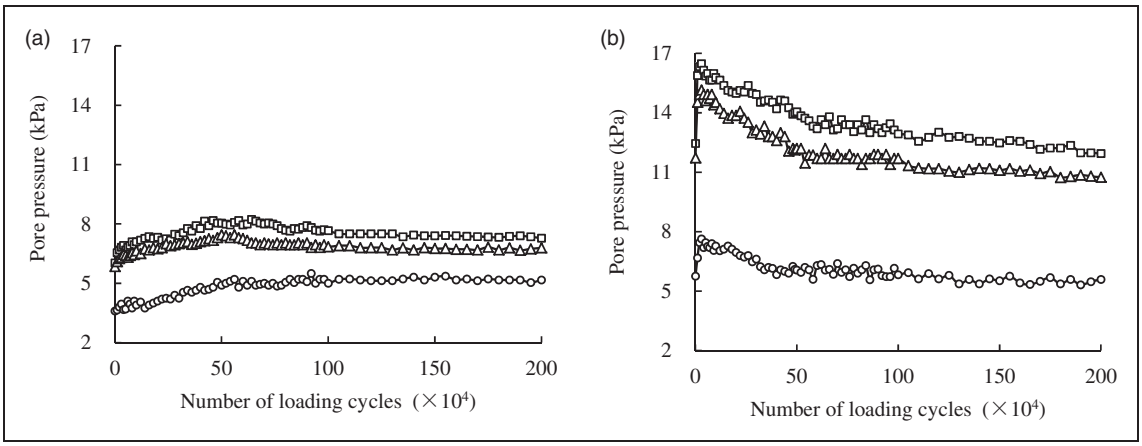


**Figure 14.** The variation of pore pressure in the subgrade bed with the number of loading cycles; □, PW-1; △, PM-2; ○, PM-3. (a) The upper layer of the subgrade bed in the normal condition; (b) the upper layer of the subgrade bed in the saturation condition.

## *Cumulative settlement*

The variation of the cumulative settlement of the upper layer of the subgrade bed with the number of loading cycles is shown in Figure 13.

When the upper layer of the subgrade bed is in the normal condition, the cumulative settlement of the subgrade bed can gradually stabilize after $5.0 \times 10^5$ cycles. After $2.0 \times 10^6$ cycles for the first loading stage, the cumulative settlement of the surface and middle position of the upper layer of the subgrade bed at the center of the model are 0.89 mm and 0.71 mm, respectively. However, once the upper layer of the subgrade bed is saturated by water, the cumulative settlement of the same measuring points in the model increases rapidly with the increasing number of loading cycles and has no convergent trend. Finally, the additional cumulative settlement of the surface and middle position of the upper layer of the subgrade bed at the center of the model is 3.22 mm and 1.92 mm, respectively. Based on the results of this full-scale model, if the upper layer of the subgrade bed is saturated by water, the subgrade bed produces new settlement under the cyclic loading, and also mud pumping occurs in the subgrade bed under the slab track structure.

## *Pore pressure*

When the upper layer of the subgrade bed in this full-scale model is in the normal and saturation conditions, the relationships between the pore pressure in the upper layer of subgrade bed and the number of loading cycles are as shown in Figure 14.

When the upper layer of the subgrade bed is in the normal condition, the pore pressure of the upper layer of the subgrade bed increases with the increasing number of loading cycles at first, and then gradually stabilizes after $5.0 \times 10^5$ cycles. While the upper layer of the subgrade bed is kept in saturation, the pore pressure of the upper layer of the subgrade bed increases rapidly at first, and then decreases gradually with the increasing number of loading cycles. Under cyclic loading, the pore pressure of each test position

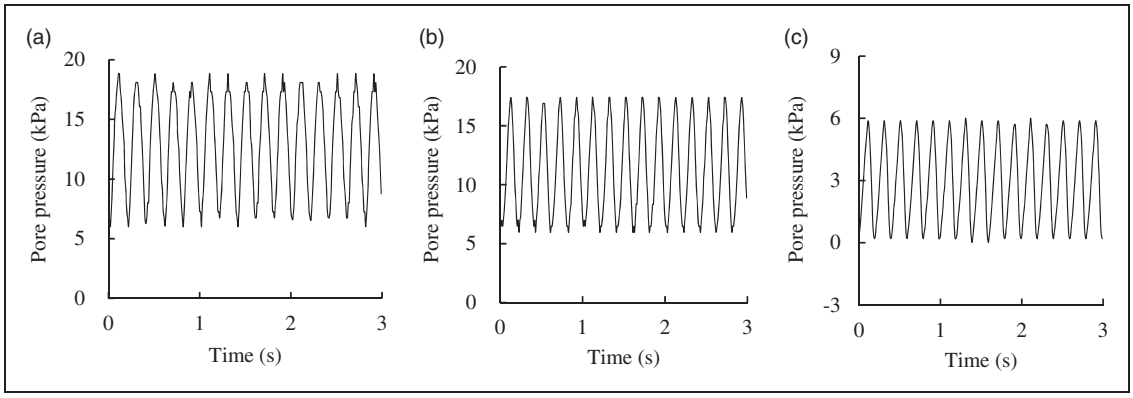


**Figure 15.** The time–history curve of the dynamic pore pressure at an advanced stage of mud pumping: (a) PW-1; (b) PW-2; (c) PW-3.

in the upper layer of the subgrade bed in saturation is more than that of the upper layer of the subgrade bed in the normal condition. When the upper layer of the subgrade bed is in the normal condition, the graded crush stone is in the unsaturated condition. The pore pressure in unsaturated soil is a complex problem and is not analyzed in this paper.

At an advanced stage of mud pumping, the time–history curve of dynamic pore pressure at different test positions is as shown in Figure 15.

When the upper layer of the subgrade bed was kept in saturation, the pore pressure at the bottom of the upper layer of the subgrade bed is more than that of the test position PW-3 near the junctures between the concrete base and waterproof layer on the subgrade bed, which can form pore pressure difference between the top and bottom surfaces of the upper layer of the subgrade bed under cyclic loading. Under the flow drive force caused by the pore pressure difference, the fine particles in the subgrade bed can be migrated upwards to the surface of the upper layer of the subgrade bed and repeatedly carried out of the subgrade bed by mud pumping, as shown in Figure 11.

## *External and internal characteristics of mud pumping*

After the completion of the first loading stage, the upper layer of the subgrade bed of the full-scale model is saturated by water and always kept in saturation during the second loading stage. Under cyclic loading, mud pumping begins to occur in the model after $3.0 \times 10^4$ cycles, and a small volume of slurry accumulates on the waterproof layer, as shown in Figure 11(a). Especially, mud pumping deteriorates gradually with the increasing number of loading cycles, which causes a large volume of slurry to be squeezed out of the subgrade bed after the completion of the second loading stage, as shown in Figure 11(b).

A waterproof layer composed of geomembrane installed between the upper and lower layers of the subgrade bed of the full-scale model has been cut off from the migration paths of fine particles from the lower layer of the subgrade bed to the upper layer of the subgrade bed. Therefore, the fine particles carried out of the subgrade bed by mud pumping are not from the lower layer of the subgrade bed but from the upper layer of the subgrade bed in this full-scale model. Combining with relevant literature,[19–24] it was concluded that mud pumping was caused by the cyclic process of pore water pressure rise-dissipation in the upper layer of the subgrade bed under dynamic loading and unloading cycle. There is a sharp rise in the pore pressure in the upper layer of the subgrade bed in the loading process of dynamic load, forming excess pore water pressure. Water infiltrates up to the surface of the upper layer of the subgrade bed under excess pore water pressure, and then flows out of the upper layer of the subgrade bed through the broken junctures between the waterproof layer and concrete base during the cyclic loading process of dynamic load. The infiltrating and flowing process of water have an instant impact force on the fine particles in the upper layer of the subgrade bed, which causes the fine particles to migrate upwards to the surface of the upper layer of the subgrade bed and be carried out of the upper layer of the subgrade bed. With the decrease of fine particles in graded crush stone, contact stress between coarse particles increases, which may cause the breakage of the contact region of some coarse particle. After the completion of the second loading stage, a large volume of slurry composed of water and fine particles is squeezed out of the subgrade bed, as shown in Figure 16.

After the completion of the second loading stage, the waterproof layer on the subgrade bed close to the concrete base is broken to form a square opening. Then the upper layer of the subgrade bed is excavated to a depth of 10 cm from the opening. It is found that there are still a large number of fine particles accumulated on the subgrade bed surface, which form a mud layer between the concrete base and subgrade bed, as shown in Figure 17. What is more, mud pumping only occurs on the surface of the subgrade bed.

Based on the external and internal characteristics of mud pumping of the full-scale model, the

supporting capability of the subgrade bed to the concrete base decreases with the increasing number of loading cycles due to the occurrence of mud pumping in the upper layer of the subgrade bed; many fine particles are carried out of the subgrade bed, and a mud layer was formed between the subgrade bed and concrete base. Therefore, the vertical vibration accelerations and displacements of the concrete base increase with the increasing number of loading cycles, while that of the subgrade bed surface decreases due to the dynamic load spreading to other areas by the concrete base.

Besides, the graded crush stone, which meets the requirements of the grain-size distribution of Chinese design specification for high-speed railways (Figure 5), is used as a filler of the upper layer of the subgrade bed in this full-scale model, and the filling quality of the subgrade bed meets the requirements of Chinese specifications for high-speed railways (Table 2). When the upper layer of the subgrade bed is in the normal condition, the vibration of the full-scale model can tend to be stable with the increasing number of loading cycles. However, when the upper layer of the subgrade bed is saturated by water and always kept in saturation during the second loading stage, mud pumping still occurs in the upper layer of the subgrade bed and gradually deteriorates with the increasing number of loading cycles. Combining the field investigations and the full-scale model testing, it is indicated that the grain-size distribution of the filler and the filling quality for the subgrade bed meet the requirements of the related specifications of high-speed railways, but mud pumping would still occur in the upper layer of the subgrade bed under long-term cyclic dynamic load, if rainwater could infiltrate into the upper layer of the subgrade bed under the slab track structure and not be quickly drained out of the upper layer of the subgrade bed. Therefore, the greater impetus for improving the long-term dynamic stability during operation should be placed on preventing water from infiltrating into the upper layer of the subgrade bed, except for strictly controlling the filler selection and filling quality of the subgrade bed in the process of design and construction of high-speed railways. Considering that it is difficult to eliminate cracks in expansion joints of the concrete base to prevent water from infiltrating into the upper layer of the subgrade bed, the subgrade bed with permeability capability through application of new materials and structural design optimization can ensure that the slab track–subgrade would not be subject to mud pumping during long-term operation.

**Figure 16.** A large volume of slurry composed of water and fine particles squeezed out of the subgrade bed.

## Conclusions and recommendations

In order to analyze the internal and external characteristics of mud pumping in the subgrade bed under the slab track structure and the influence of mud pumping in the subgrade bed on the dynamic properties of the slab track–subgrade, various field investigations were conducted and a full-scale model was established. The results based on the field investigations and the full-scale model testing can be summarized as follows:

(1) Mud pumping only occurs at the expansion joints in the concrete base of the slab track structure, due to cracks in the expansion joints of the

**Figure 17.** The internal characteristics of mud pumping in the upper layer of the subgrade bed.

concrete base caused by waterproof materials aging in the expansion joints. Rainwater can infiltrate into the upper layer of subgrade bed through the cracks, which causes the upper layer of the subgrade bed to be filled with the graded crush stone affected by dynamic fluid–solid coupling effects under high-speed moving train loads. Besides, a large number of fine particles are carried out of the subgrade bed once mud pumping occurs in the subgrade bed during operation.

(2) When the upper layer of the subgrade bed is in the normal condition, the full-scale model of the slab track–subgrade has a good long-term dynamic stability under the cyclic loading. However, when the upper layer of the subgrade bed is saturated by water and always kept in saturation, mud pumping begins to occur in the upper layer of subgrade bed after $3.0 \times 10^4$ cycles and deteriorates rapidly with the increasing number of loading cycles, which causes a large number of fine particles to be squeezed out of the subgrade bed. At the same time, the vertical vibration acceleration and displacement of the concrete base increase quickly at first and then increase gradually, and that of the subgrade surface decrease gradually, with the continual increase of the cumulative settlement of the upper layer of the subgrade bed. What is more, the occurrence of mud pumping in the subgrade bed can enlarge the ratio of the vibration acceleration and displacement of the subgrade bed to that of the concrete base of the slab track structure, due to the reduction of the supporting capability of the subgrade bed to the slab track structure caused by mud pumping in the subgrade bed.

(3) Mud pumping can still occur in the subgrade bed under the cyclic dynamic load if rainwater could infiltrate into and not be quickly drained out of the subgrade bed, although the filler selection and filling quality of the upper layer of the subgrade bed meet the requirements of design specification of high-speed railway. With the deterioration of mud pumping in the subgrade bed, the external characteristics of mud pumping of the slab track–subgrade are that the fine particles can be continually carried out of the subgrade bed, and the internal characteristics are that mud pumping only occurs on the surface of the subgrade bed under the concrete base and forms a mud layer between the subgrade bed and concrete base, thereby causing the reduction of the supporting capability of the subgrade bed to the slab track structure, which affects the comfort and safety of operation of high-speed railways.

Therefore, in order to prevent mud pumping from occurring in the slab track–subgrade, more attention should be given on the waterproofing and drainage design of the subgrade bed to prevent water from infiltrating into the subgrade bed under the slab track structure. If rainwater could infiltrate into the subgrade bed through the cracks in the slab track structure, it must be able to be quickly drained out of the subgrade bed to avoid the filler of the subgrade bed being affected by the coupling effects of rainwater and dynamic load under high-speed moving train loads.

## Declaration of Conflicting Interests

The author(s) declared no potential conflicts of interest with respect to the research, authorship, and/or publication of this article.

## Funding

The author(s) disclosed receipt of the following financial support for the research, authorship, and/or publication of this article: This study was supported by the National Natural Science Foundation of China (Grant nos. 51508478 and 5178467), the Technology Research and Development Program of Chinese Railway Corporation (Grant no. 2016G002–E), and the National Key Research and Development Program of China (Grant no. 2017YFB1201204-052).

## ORCID iD

Junjie Huang http://orcid.org/0000-0002-6901-3374

## References

1. Ren JJ, Yang RS, Wang P, et al. Influence of contact loss underneath concrete underlayer on dynamic performance of prefabricated concrete slab track. *Proc IMechE, Part F: J Rail and Rapid Transit* 2017; 234: 345–358.
2. Zhang X, Burrow M and Zhou S. An investigation of subgrade differential settlement on the dynamic response of the vehicle–track system. *Proc IMechE, Part F: J Rail and Rapid Transit* 2016; 230: 1760–1773.
3. Pita AL, Teixeira PF and Robusté F. High speed and track deterioration: the role of vertical stiffness of the track. *Proc IMechE, Part F: J Rail and Rapid Transit* 2004; 218: 31–40.
4. Lei X and Zhang B. Influence of track stiffness distribution on vehicle and track interactions in track transition. *Proc IMechE, Part F: J Rail and Rapid Transit* 2010; 224: 592–604.
5. Zhai W, He ZX and Song XL. Prediction of high-speed train induced ground vibration based on train-track-ground system model. *Earthq Eng Eng Vib* 2010; 9: 545–554.
6. Zhai WM and Sun XL. A detailed model for investigating vertical interaction between railway vehicle and track. *Veh Syst Dyn* 1994; 23: 603–615.
7. Zhai WM, Wang KY and Cai CB. Fundamentals of vehicle–track coupled dynamics. *Veh Syst Dyn* 2009; 47: 1349–1376.
8. Lei XY and Mao LJ. Dynamic response analyses of vehicle and track coupled system on track transition of conventional high speed railway. *J Sound Vib* 2004; 271: 1133–1146.
9. Chen RP, Wang ZZ, Jiang HG, et al. Experimental study of dynamic load magnification factor. *Rock Soil Mech* 2013; 34: 1045–1052.
10. Chen RP, Zhao X, Wang ZZ, et al. Experimental study on dynamic load magnification factor for ballastless

track-subgrade of high-speed railway. *J Rock Mech Geotech Eng* 2013; 5: 306–311.
11. Su Q and Cai Y. A spatial time-varying coupling model for dynamic analysis of high speed railway subgrade. *J Southwest Jiaotong Univ* 2001; 36: 509–513.
12. Bian XC, Jiang HG, Cheng CM, et al. Full-scale model testing on a ballastless high-speed railway under simulated train moving loads. *Soil Dyn Earthq Eng* 2014; 66: 368–384.
13. Correia dos Santos N, Barbosa J, Calcada R, et al. Track-ground vibrations induced by railway traffic: experimental validation of a 3D numerical model. *Soil Dyn Earthq Eng* 2017; 97: 324–344.
14. Liang B, Zhu D and Cai Y. Dynamic analysis of the vehicle–subgrade model of a vertical coupled system. *J Sound Vib* 2001; 245: 79–92.
15. Zhao CY and Ping W. Minimizing noise from metro viaduct railway lines by means of elastic mats and fully closed noise barriers. *Proc IMechE Part F: J Rail and Rapid Transit* 2018; 232: 1828–1836.
16. Connolly DP, Costa PA, Kouroussis G, et al. Large scale international testing of railway ground vibrations across Europe. *Soil Dyn Earthq Eng* 2015; 71: 1–12.
17. Popp K, Schiehlen W, et al. *System dynamics and long-term behaviour of railway vehicles, track and subgrade*. New York: Springer Science & Business Media, 2013.
18. Bezin Y, Farrington D, Penny C, et al. The dynamic response of slab track constructions and their benefit with respect to conventional ballasted track. *Veh Syst Dyn* 2010; 48: 175–193.
19. Alobaidi I and Hoare D. Factors affecting the pumping of fines at the subgrade subbase interface of highway pavements: a laboratory study. *Geosynth Int* 1994; 1: 221–259.
20. Alobaidi I and Hoare D. Development of pore water pressure at the subgrade-subbase interface of a highway pavement and its effect on pumping of fines. *Geotext Geomembr* 1996; 14: 111–135.
21. Alobaidi I and Hoare D. Mechanisms of pumping at the subgrade-subbase interface of highway pavements. *Geosynt Int* 1999; 6: 241–259.
22. Boomintahan S and Srinivasan GR. Laboratory studies on mud pumping into ballast under repetitive rail loading. *Indian Geotech J* 1988; 18: 31–47.
23. Ayres DJ. Geotextiles or geomembranes in track? British Railways' experience. *Geotext Geomembr* 1986; 3: 129–142.
24. Duong TV, Cui YJ, Tang AM, et al. Investigating the mud pumping and interlayer creation phenomena in railway sub-structure. *Eng Geol* 2014; 171: 45–58.
25. Alobaidi I and Hoare D. Qualitative criteria for anti-pumping geocomposites. *Geotext Geomembr* 1998; 16: 221–245.
26. Hudson A, Watson G, Le Pen L, et al. Remediation of mud pumping on a ballasted railway track. *Procedia Eng* 2016; 143: 1043–1050.
27. Chawla S and Shahu JT. Reinforcement and mud-pumping benefits of geosynthetics in railway tracks: numerical analysis. *Geotext Geomembr* 2016; 44: 344–357.
28. Chawla S and Shahu JT. Reinforcement and mud-pumping benefits of geosynthetics in railway tracks: model tests. *Geotext Geomembr* 2016; 44: 366–380.
29. Machii K. Mud pumping on tracks – present state and countermeasures. *Japanese Railw Eng* 1978; 17: 20–21.
30. Li D and Selig E. Method for railway track foundation design. *J Geotech Geoenviron Eng* 1998; 124: 316–329.
31. Hayashi S and Shahu JT. Mud pumping problem in tunnels on erosive soil deposits. *Geotechnique* 2000; 50: 393–408.
32. Zhang WC, Su Q, Liu T, et al. Research on vibration characteristics of ballastless track subgrade under frost boiling at subgrade bed. *Rock Soil Mech* 2014; 35: 3556–3568.
33. Liu T, Su Q, Zhao WH, et al. Study on injection-repaired and reinforcement effects of subgrade frost boiling under ballastless track. *J China Railw Soc* 2015; 37: 88–95.
34. Zhiyuan Z. Subgrade mudding analysis and treatment measures of Shanghai-Nanjing intercity railway. *Railw Eng* 2014; 3: 74–77.
35. Huang JJ, Su Q, Wang W, et al. Vibration behavior and reinforcement effect analysis of the slab track-subgrade with mud pumping under cyclic dynamic loading: full-scale model tests. *Shock Vib* 2018; 2018: 1–14. DOI: 10.1155/2018/3087254.
36. Yuan R. The study on railway mud pumping and management of Japan. *Dev Railw Sci Technol* 1979; 4: 16–18.
37. Ministry of Railways of the People's Republic of China. *TB 10621–2014: Code for design of high speed railway*. Beijing: China Railway publishing House, 2015.
38. Hu YF and Li NF. *Theory of ballastless track-subgrade for high speed railway*. Beijing: China Railway Publishing House, 2010.
39. Huang JJ, Su Q, Zhao WH, et al. Experimental study on use of lightweight foam concrete as subgrade bed filler of ballastless track. *Constr Build Mater* 2017; 149: 911–920.
40. Huang JJ, Su Q, Liu T, et al. Vibration and long-term performance analysis of pile-plank-supported low subgrade of ballastless track under excitation loads. *Shock Vib* 2015; 2015: 1–12.
41. Liu XH, Yang GL and Wang LL. Dynamic response testing and analysis on red-clay cutting bed under ballastless track of high-speed railway. *Geotech Invest Survey* 2011; 39: 12–18.
42. Liu G, Luo Q, Zhang L, et al. Analysis on the dynamic stress characteristics of the unballasted track subgrade under train loading. *J China Railw Soc* 2013; 35: 86–93.
43. Jiang HG, Bian XC, Xu X, et al. Full-scale model tests on dynamic performances of ballastless high-speed railways under moving train loads. *Chinese J Geotech Eng* 2014; 36: 354–362.
44. Jol HM. *Ground penetrating radar theory and applications*. Amsterdam: Elsevier Science, 2009.
45. Soldovieri F, Persico R, Utsi E, et al. The application of inverse scattering techniques with ground penetrating radar to the problem of rebar location in concrete. *NDT & E Int* 2006; 39: 602–607.
46. Benedetto A, Tosti F, Ciampoli LB, et al. An overview of ground-penetrating radar signal processing techniques for road inspections. *Signal Process* 2017; 132: 201–209.
47. Shangguan P, Al-Qadi I, Coenen A, et al. Algorithm development for the application of ground-penetrating

radar on asphalt pavement compaction monitoring. *Int J Pavement Eng* 2016; 17: 189–200.
48. Zhang JK, Yan W and Cui DM. Concrete condition assessment using impact-echo method and extreme learning machines. *Sensors* 2016; 16: 447.
49. Hsieh CT and Lin Y. Detecting debonding flaws at the epoxy–concrete interfaces in near-surface mounted CFRP strengthening beams using the impact–echo method. *NDT & E Int* 2016; 83: 1–13.
50. Ministry of Railways of the People's Republic of China. *TB 10102–2010: Code for soil test of railway engineering*. Beijing: China Railway Publishing House, 2010.